Supplemental Material

Schwanghart, W., and Scherler, D., 2020, Divide mobility controls knickpoint migration on the Roan Plateau (Colorado, USA): Geology, v. 48, https://doi.org/10.1130/G47054.1

Divide mobility controls knickpoint migration on the Roan Plateau (Colorado, USA)

Wolfgang Schwanghart[1*], Dirk Scherler[2,3]

[1]*Institute of Environmental Science and Geography, University of Potsdam, 14476 Potsdam, Germany*

[2]*German Research Centre for Geosciences (GFZ), Earth Surface Geochemistry, 14473 Potsdam, Germany*

[3]*Institute of Geological Sciences, Freie Universität Berlin, 12249 Berlin, Germany*

**E-mail: w.schwanghart@geo.uni-potsdam.de*

SUPPLEMENTARY METHODS

Digital elevation model

We used the 1-arcsecond digital elevation models (DEMs) from the Shuttle Radar Topography Mission (SRTM) (Jarvis et al., 2008) and ALOS 3D World DEM (Takaku et al., 2014), projected 30 m resolution (UTM WGS84 Zone 12), as topographic data for our analysis. The SRTM DEM features numerous missing values as well as errors that we filled and corrected with the ALOS 3D World DEM. Based on the DEM and flow directions obtained with TopoToolbox (Schwanghart and Scherler, 2014), we derived the stream network with a minimum supporting drainage area of 0.18 km^2 which refers to 200 pixels in the DEM.

Knickpoint identification

The Parachute Creek dissects the Roan Plateau (Berlin and Anderson, 2007). Headward incision occurs along vertical-step knickpoints (Whipple et al., 2013), which separate the relict landscape from the up to 500-800 m lower bottoms of incised canyons. These knickpoints are pronounced convex sections in otherwise concave-upward river profiles. Following preprocessing of the stream network using quantile carving (quantile τ=0.5) (Schwanghart and Scherler, 2017), we identified knickpoints with an automated procedure implemented in TopoToolbox (function *knickpointfinder*) and described in Stolle et al. (2019). The procedure adjusts a strictly upward concave profile to the actual river profile by relaxing the curvature constraint at locations (knickpoints) where the vertical distance between the modelled and the actual profile attains a maximum value. The procedure is repeated until the maximum vertical distance is less than a tolerance value which either reflects river profile uncertainty or the minimal knickpoint height. We chose a tolerance value of 70 m which resulted in 103 knickpoints in the Parachute Creek basin (Figure S1). Visual crosschecking showed that all identified knickpoints are related to the upper ledge of the Roan Plateau.

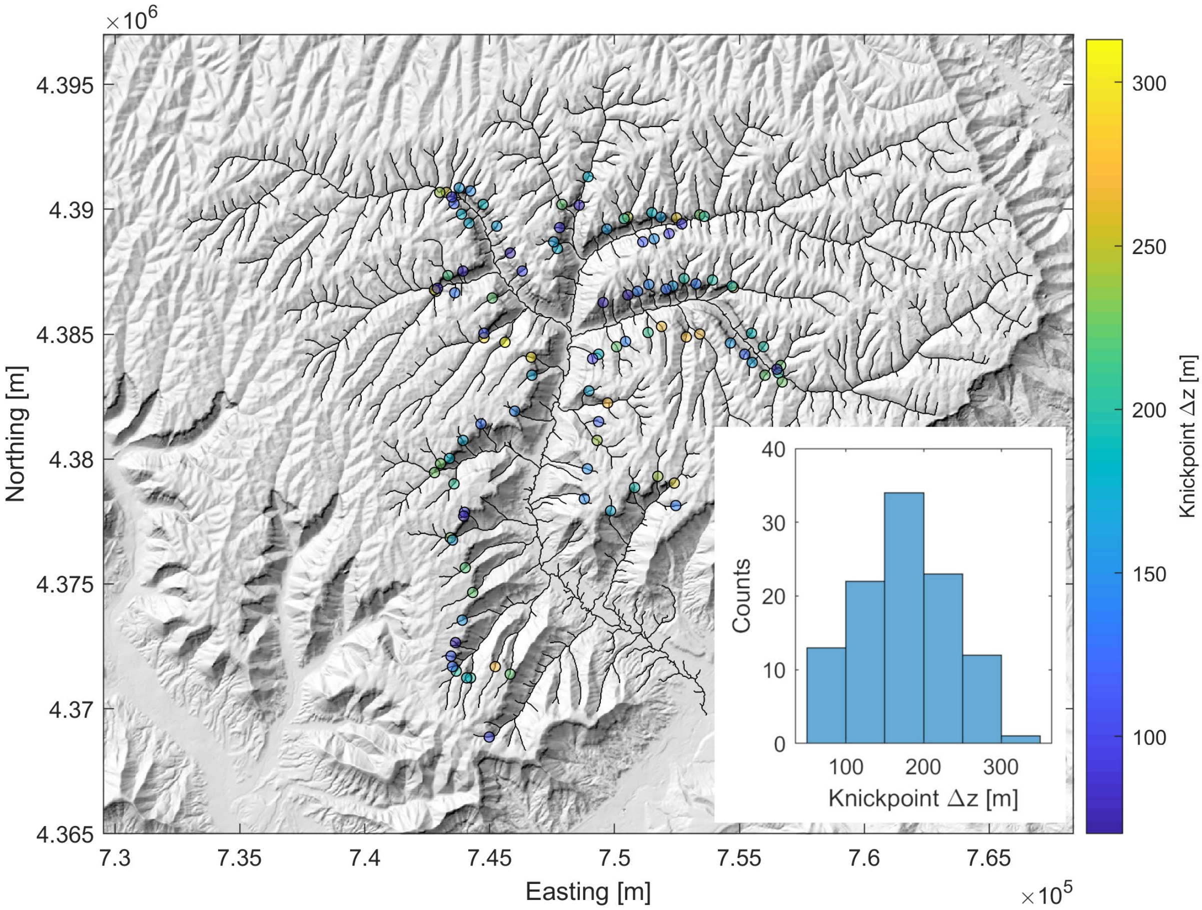

Figure S1: Spatial distribution of knickpoints and knickpoint heights (Δz) in the Parachute Creek basin.

Determination of stream power parameters

Commonly, the river-profile concavity (or m/n ratio) is in the range 0.3-1.2 (Whipple et al., 2013), but its actual value for a given river is typically unknown. In a steady state landscape with spatially invariant rock uplift, the m/n-ratio can be found by maximizing the correlation coefficient between χ and elevation, that is, where the river profile attains a linear shape in χ-space (Perron and Royden, 2013). However, if assumptions (spatially invariable K and U, topographic steady state) are violated, deriving the m/n ratio is more challenging. An approach which is less sensitive to deviations from perfectly graded rivers detects optimal values of the m/n-ratio by maximizing the collinearity of χ of all streams in a network using rank statistics (Hergarten et al., 2016). If rivers traverse regions with different uplift rates or erosional efficiencies, piecewise regression techniques have also been used (Mudd et al., 2014). An alternative approach that is particularly suited to account for transient scenarios of river profile evolution has been developed by Goren et al. (2014).

Here we apply a different approach to determining both the m/n-ratio as well as K. Based on numerous geochronological constraints (see references in Berlin and Anderson (2007)), knickpoints in the Parachute Creek basin emanated from a common base level fall at the Parachute Creek basin outlet at $t_0 = 8$ Ma. For a linear stream power model ($n = 1$), knickpoint celerity is proportional to upstream area to the exponent m (Berlin and Anderson, 2007; Fox et al., 2014).

$$\frac{dx}{dt} = KA(x)^m \tag{1}$$

According to this model, the response time τ of a particular location x in the stream network is calculated by

$$\tau(x) = \int_{x=0}^{x} \frac{1}{KA(x)^m} dx \tag{2}$$

Acknowledging that τ is inversely proportional to K enables us to introduce the variable χ [m]

$$\chi = A_0^m K\tau \tag{3}$$

According to the stream-power incision model, knickpoint locations should cluster in a narrow range of χ values, if the knickpoints derive from a common base-level fall (Royden and Perron, 2013). With t_0 known, we can solve Eq. 3 for m and K by minimizing the variability of knickpoint χ values χ_{kp}.

$$\min_{m,K}\left(\sum\left(\frac{\chi_{kp}}{KA_0^m} - t_0\right)^2\right) \tag{4}$$

We solve Eq. 4 using a Levenberg-Marquardt nonlinear least squares algorithm (MATLAB function *nlinfit*). The estimated variance-covariance matrix shows a strong correlation between the parameters and indicates that a previous estimate of m and K by Berlin and Anderson (2007) is located on the major axis of the covariance ellipse (Figure S2).

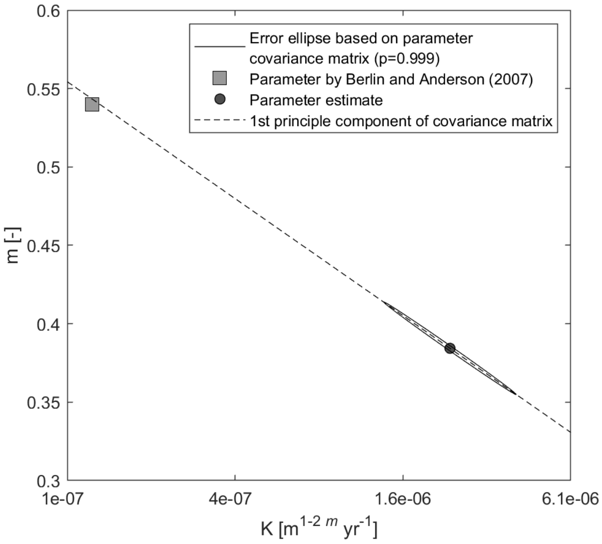

Figure S2: Optimal value and uncertainties of m and K that minimize the variability of knickpoint χ values in the Parachute Creek basin without the East Fork creek. A previous estimate of Berlin and Anderson (2007) for the Roan Plateau (Roan and Parachute Creek) had a higher value of m and lower value of K.

Divides

We calculated divides based on the flow directions derived from the DEM. The divides have variable morphologies which we quantitatively describe using the hillslope relief asymmetry metric (Scherler and Schwanghart, 2019). The metric calculates the ratio between hillslope relief on either side of the divide. The resulting map is shown in Figure S3. Divides that coincide with the margin of the Roan

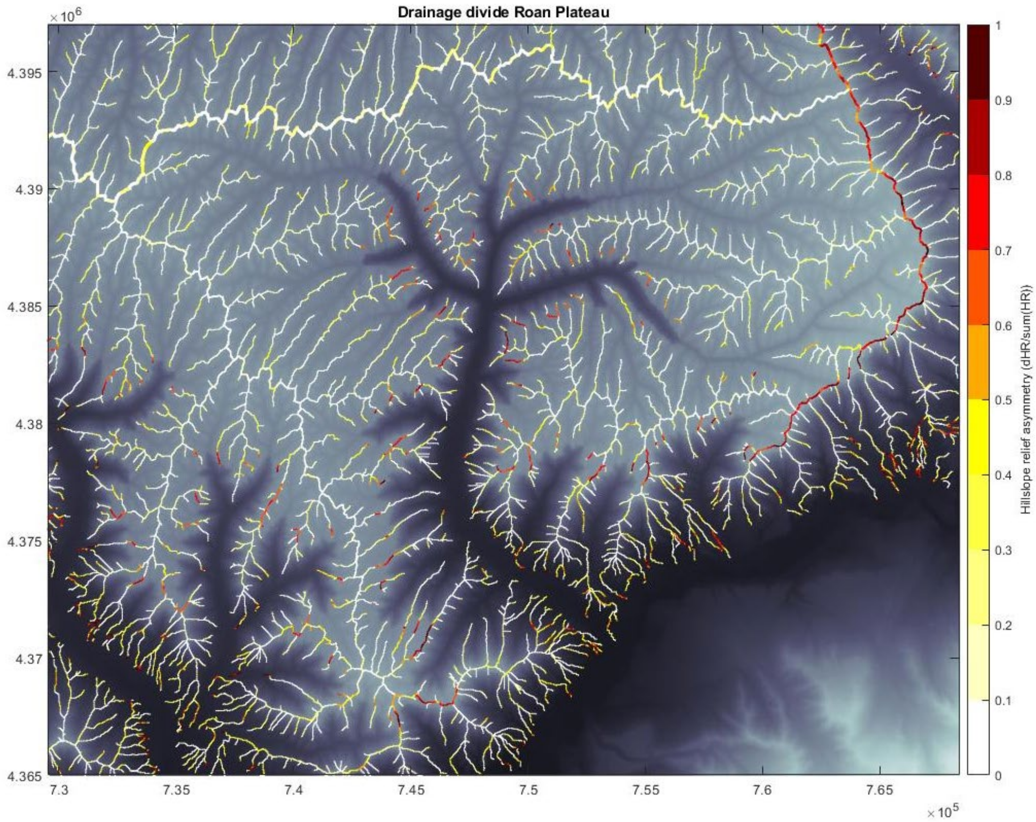

Figure S3: Hillslope relief asymmetry in the Parachute Creek basin.

Plateau show particularly high values.

Distribution of knickpoint χ-values

Knickpoint χ-values (χ_{kp}) in the Parachute Creek basin exhibit a peaked distribution (Fig. 1D). They vary between $\chi = 2900$ and 4300 m (about a tenth of the entire range of χ in the Parachute Creek basin), with an average value of 3600 m. The spatial distribution of χ_{kp} shows that there are consistent patterns of either high or low values in tributaries to the Parachute Creek with particularly pronounced deviations in the East Fork subbasin (Figure S4). Median χ_{kp} in the East Fork subbasin are higher compared to the other subbasins (significantly different at the 5% significance level).

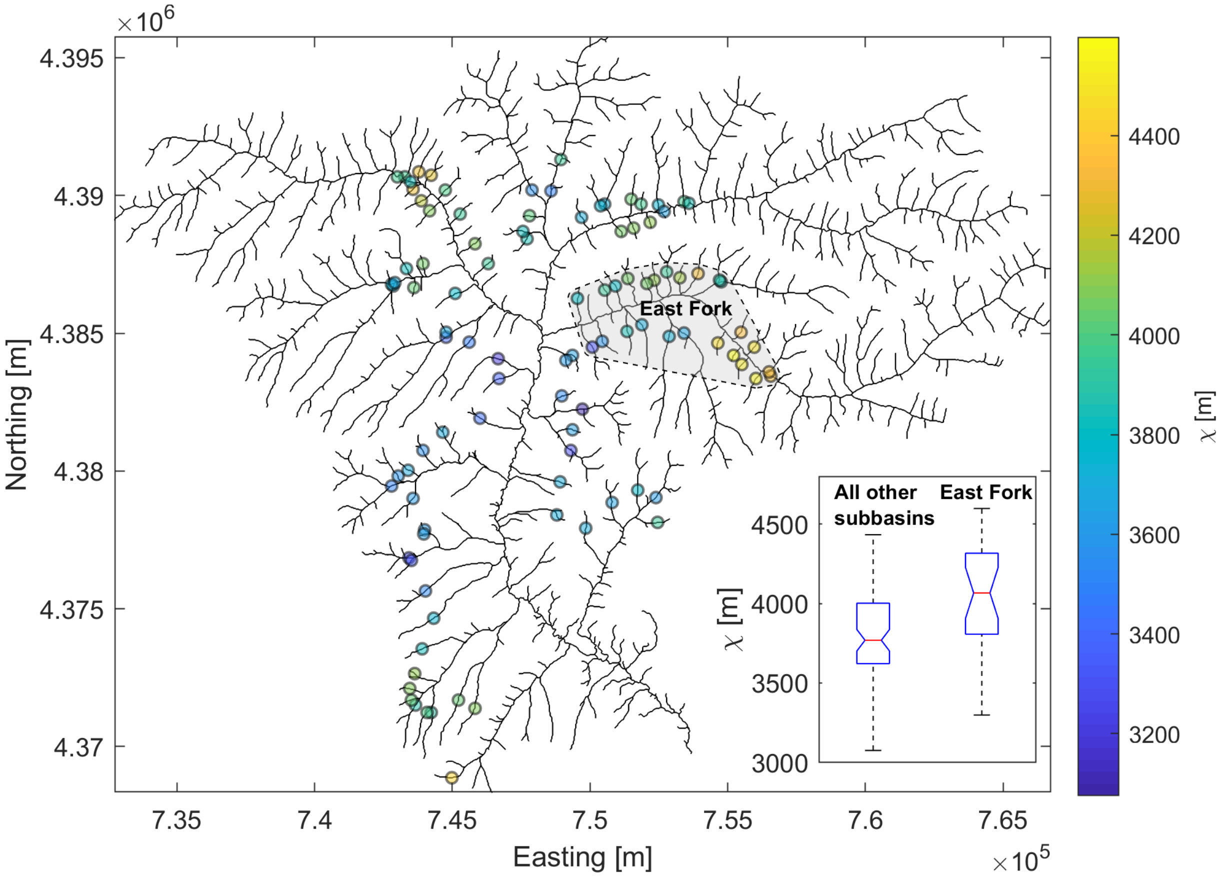

Figure S4: Knickpoints in the Parachute Creek basin. Knickpoint coloring is according to χ-values measured along the stream network using a m/n-ratio of 0.40 and a reference area $A_0 = 1x10^6$ m^2. Knickpoint χ-values in the East Fork subbasin are generally higher than those of the remaining subbasins of the Parachute Creek basin.

Constraints on area-loss in the East Fork subbasin

The variable χ is a function of upslope area (see Eq. 2 and 3). By adjusting the upslope area, we can potentially reduce the scatter in χ_{kp}. To determine potential changes in area in the East Fork subbasin, we used the same approach as above, i.e. minimizing the variability of χ_{kp}. However, this time we kept m and K constant, but varied the upstream area. Note that upstream area is calculated by solving the continuity equation of network flow (Strang, 1988; Ahuja et al., 1993; Schwanghart and Kuhn, 2010), that in matrix notation is written as

$$\boldsymbol{a} = \left(\boldsymbol{I} - \boldsymbol{M}^{\boldsymbol{T}}\right)^{-1} \boldsymbol{w} \tag{5}$$

$\boldsymbol{a}$ is a $nx1$ vector with upslope areas for each of the n pixels in the DEM, $\boldsymbol{I}$ is the nxn identity matrix, and $\boldsymbol{M}$ is the nxn transfer matrix (Schwanghart and Kuhn, 2010) or adjacency matrix of the directed flow network (Heckmann et al., 2015) and $\boldsymbol{T}$ indicates its transpose. $\boldsymbol{w}$ is a vector with the rates with which water enters the system in every pixel. When calculating upslope area, this rate is usually set as pixel area which is then accumulated downstream by Eq. 5. A vector with χ values is accordingly calculated by

$$\boldsymbol{\chi} = (\boldsymbol{I} - \boldsymbol{M})^{-1} \left(\frac{A_0}{(\boldsymbol{I} - \boldsymbol{M}^{\boldsymbol{T}})^{-1} \boldsymbol{w}} \boldsymbol{\Delta x} \right) \tag{6}$$

where $\boldsymbol{\Delta x}$ is a $nx1$ vector where each element refers to a distance of each pixel to its downstream neighboring pixel. Modifying the area at a specific element i in $\boldsymbol{w}$ allows us to increase or decrease upstream area while calculating χ. We select a pixel at x=766733 m and y = 4387345 m in the East Fork subbasin and run the optimization scheme

$$\min_{w_i} \left(\sum \left(\frac{\chi_{kp}}{K A_0^m} - t \right)^2 \right) \tag{7}$$

Resulting estimates of area loss are prone to errors due to the variability of χ_{kp}, but also due to uncertainties in K and m. To propagate these uncertainties to the estimates of area loss, we randomly sampled (n_r = 100) the bivariate Gaussian probability distributions of m and $\log(K)$ as obtained from our nonlinear model fit. Using the random samples of m and K, we repeated our optimization method to determine area loss. Using 1000 random samples of the probability distributions of each of the n_r area estimates were subsequently used to determine confidence intervals that include the propagated uncertainties in K and m.

Determination of area-changes in multiple subbasins of the Parachute Creek

Adding or removing drainage area at one location effects χ_{kp} values along all streams in the drainage basin. Moreover, our previous approach neglects that additional loss or gain might have occurred in other subbasins, too. Thus, in a second approach, we manually selected three more locations with variable drainage areas. We focused on the heads of the main tributaries to the Parachute Creek to avoid a too-large number of parameters and possibly poor convergence of the optimization scheme. Using the selected locations, we reran the nonlinear optimization (Eq. 7) with now four free parameters. The results of the optimization are shown in Figure S5.

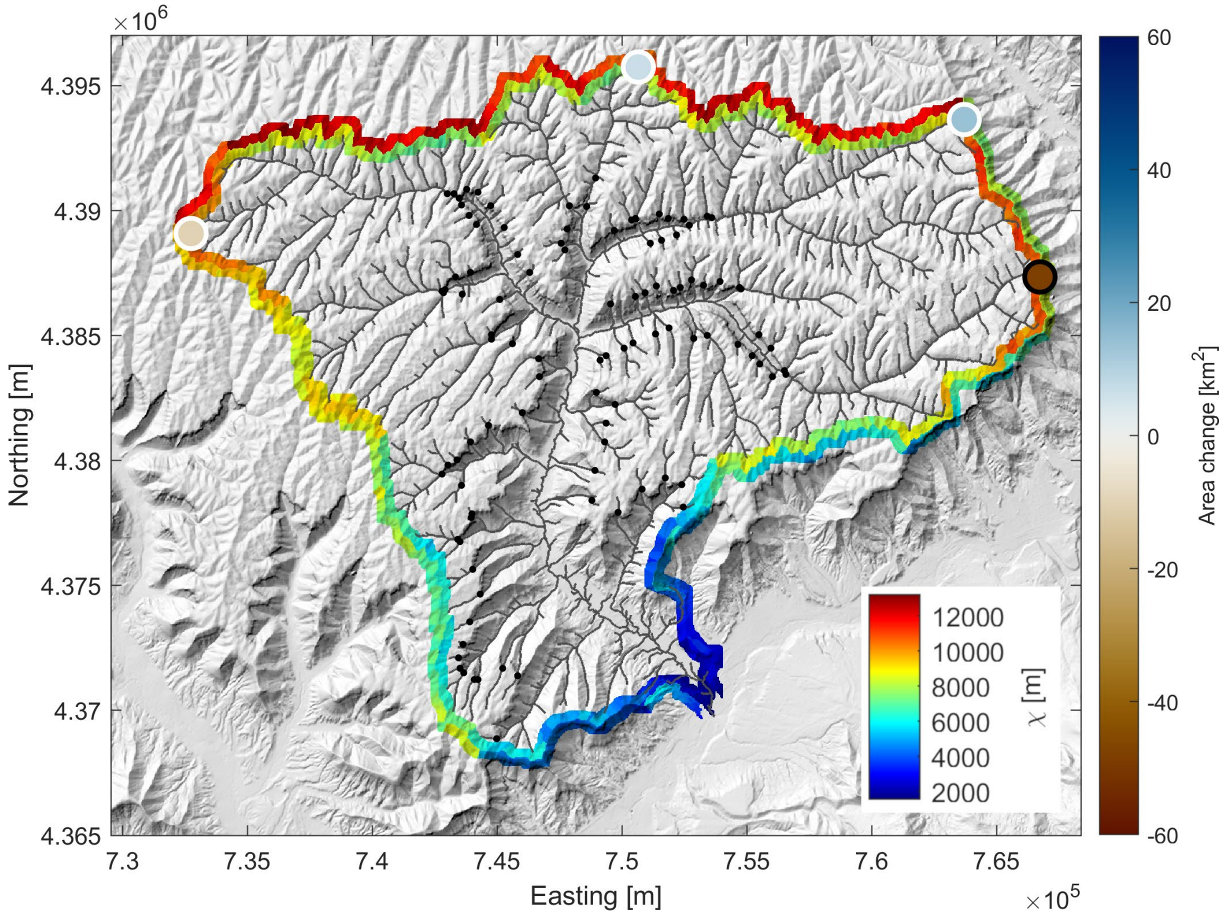

Figure S5: Determination of potential losses and gains in drainage areas at selected locations (colored circles) in the Parachute Creek basin based on minimizing the variability of χ values at knickpoint locations (black dots). Black lines show the stream network. Coloring of the circles is according to modelled area changes and black outlines indicate locations where modelled area changes have confidence intervals (95%) that exclude zero area change. Confidence intervals are obtained from the Jacobian of nonlinear regression model. The divide of the Parachute Creek is colored using the nearest χ values of channelheads on either side of the divide. Different values on either side indicate potential divide movements from lower values to higher values of χ. Colormaps in the figure are taken from Scientific Colour Maps (Crameri, 2018).

Constraining the timing and amount of area changes

To assess the dynamics and timing of divide migration, we developed a Lagrangian model of knickpoint migration along the network of the Parachute Creek basin. The model solves Eq. 2, but allows drainage area A to be variable in time and space:

$$\frac{dx}{dt} = KA(x,t)^m \tag{8}$$

The model simulates a knickpoint that is initiated upon base level drop at the Parachute Creek outlet at 8 Ma. The knickpoint subsequently migrates upstream at velocities that we calculate using Eq. 8. Values of K and m are as determined above, and are assumed to be constant in time and space. While migrating upstream, the knickpoint is cloned at confluences from where knickpoints propagate into tributaries. The numerical implementation takes the present-day flow network but is meshfree in space because knickpoints are allowed to be located at fractions of edges between nodes of the network. However, we numerically solve Eq. 8 in time using time steps of 10,000 years, which allows us to simulate different scenarios of area loss in the East Fork subbasin.

In total, we carried out 420 simulations in which we vary the area lost in the East Fork subbasin as well as the onset of area-loss. In all simulations we assume a constant rate of area loss upon onset until the upstream area in the East Fork subbasin equals the present-day catchment area. The 420 simulations are run with 20 different initial additional areas equally spaced between 0 and 200 km^2 in the East Fork subbasin as well as 21 different onsets of area-loss equally spaced between 6 Ma (2 Ma following incision at the Parachute Creek outlet) and present day.

Assessing the simulations requires a method that compares the actual and simulated knickpoints on the network. Our comparison relies on spatial kernel density estimates of the actual knickpoint patterns on the stream network. We obtained these estimates using the method of McSwiggan et al. (2017) which calculates kernel densities around the actual knickpoints by solving the heat equation on the stream network (Figure S6) and thus emulates a Gaussian kernel density estimator. This approach should be preferred over the commonly used summation of kernel-density estimates on the one-dimensional lines because it preserves probability mass at network junctions (Okabe et al., 2009; Okabe and Sugihara, 2012; Baddeley et al., 2015; McSwiggan et al., 2017). The diffusivity coefficient of the heat equation was chosen so that the resulting bandwidth of the kernel equals 300 m.

We assessed the goodness-of-fit by summing the kernel densities at the locations of the simulated knickpoints (Figure S6). To this end, we took the sum of the log-densities of all simulated knickpoints as target function to evaluate how well simulated knickpoints correspond to the actual ones.

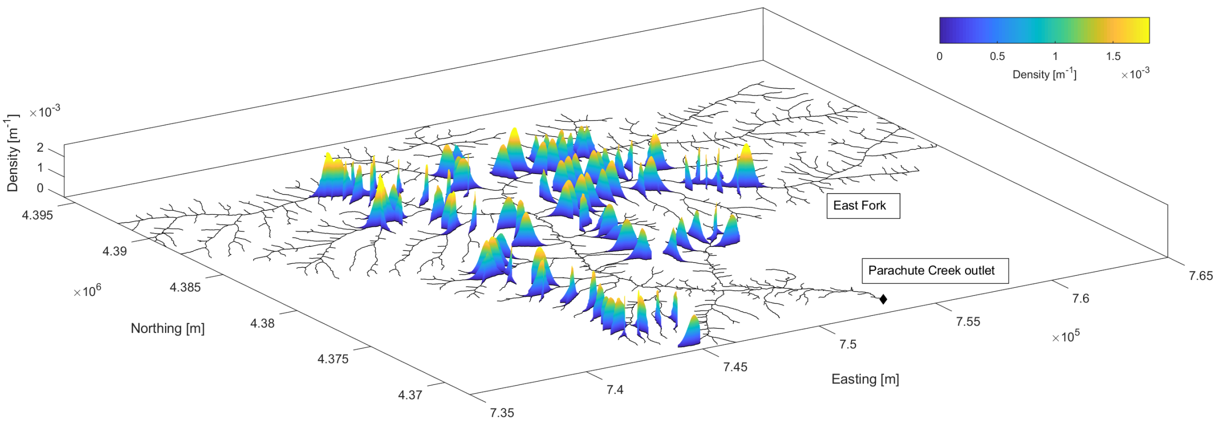

Figure S6: 3D visualization of the kernel density estimate of the spatial distribution of actual knickpoints on the flow network. The black diamond shows the outlet of the basin.

SUPPLEMENTAL REFERENCES

Ahuja, R.K., Magnanti, T.L., and Orlin, J.B., 1993, Network flows: theory, algorithms, and applications: Prentice Hall, 870 p.

Baddeley, A., Rubak, E., and Turner, R., 2015, Spatial Point Patterns: Methodology and Applications with R: Boca Raton ; London ; New York, Apple Academic Press Inc., 810 p.

Berlin, M.M., and Anderson, R.S., 2007, Modeling of knickpoint retreat on the Roan Plateau, western Colorado: Journal of Geophysical Research: Earth Surface, v. 112, doi:10.1029/2006JF000553.

Crameri, F., 2018, Geodynamic diagnostics, scientific visualisation and StagLab 3.0: Geoscientific Model Development, v. 11, p. 2541–2562, doi:https://doi.org/10.5194/gmd-11-2541-2018.

Fox, M., Goren, L., May, D.A., and Willett, S.D., 2014, Inversion of fluvial channels for paleorock uplift rates in Taiwan: Journal of Geophysical Research: Earth Surface, v. 119, p. 1853–1875, doi:10.1002/2014JF003196.

Goren, L., Fox, M., and Willett, S.D., 2014, Tectonics from fluvial topography using formal linear inversion: Theory and applications to the Inyo Mountains, California: Journal of Geophysical Research: Earth Surface, v. 119, p. 1651–1681, doi:10.1002/2014JF003079.

Heckmann, T., Schwanghart, W., and Phillips, J.D., 2015, Graph theory—Recent developments of its application in geomorphology: Geomorphology, v. 243, p. 130–146, doi:10.1016/j.geomorph.2014.12.024.

Hergarten, S., Robl, J., and Stüwe, K., 2016, Tectonic geomorphology at small catchment sizes – extensions of the stream-power approach and the χ method: Earth Surface Dynamics, v. 4, p. 1–9, doi:10.5194/esurf-4-1-2016.

Jarvis, A., Reuter, H.I., Nelson, A., and Guevara, E., 2008, Hole-filled seamless SRTM data V4:

McSwiggan, G., Baddeley, A., and Nair, G., 2017, Kernel Density Estimation on a Linear Network: Scandinavian Journal of Statistics, v. 44, p. 324–345, doi:10.1111/sjos.12255.

Mudd, S.M., Attal, M., Milodowski, D.T., Grieve, S.W.D., and Valters, D.A., 2014, A statistical framework to quantify spatial variation in channel gradients using the integral method of channel profile analysis: Journal of Geophysical Research: Earth Surface, v. 119, p. 2013JF002981, doi:10.1002/2013JF002981.

Okabe, A., Satoh, T., and Sugihara, K., 2009, A kernel density estimation method for networks, its computational method and a GIS-based tool: International Journal of Geographical Information Science, v. 23, p. 7–32, doi:10.1080/13658810802475491.

Okabe, A., and Sugihara, K., 2012, Spatial analysis along networks: statistical and computational methods: Chicheser, John Wiley & Sons, Statistics in practice, 288 p.

Perron, J.T., and Royden, L., 2013, An integral approach to bedrock river profile analysis: Earth Surface Processes and Landforms, v. 38, p. 570–576, doi:10.1002/esp.3302.

Royden, L., and Perron, J.T., 2013, Solutions of the stream power equation and application to the evolution of river longitudinal profiles: Journal of Geophysical Research, v. 118, p. 1–22.

Scherler, D., and Schwanghart, W., 2019, Identification and ordering of drainage divides in digital elevation models: Earth Surface Dynamics Discussions, p. in review (open discussion esurf-2019-51).

Schwanghart, W., and Kuhn, N.J., 2010, TopoToolbox: A set of Matlab functions for topographic analysis: Environmental Modelling & Software, v. 25, p. 770–781, doi:10.1016/j.envsoft.2009.12.002.

Schwanghart, W., and Scherler, D., 2017, Bumps in river profiles: uncertainty assessment and smoothing using quantile regression techniques: Earth Surface Dynamics, v. 5, p. 821–839, doi:10.5194/esurf-5-821-2017.

Schwanghart, W., and Scherler, D., 2014, TopoToolbox 2 – MATLAB-based software for topographic analysis and modeling in Earth surface sciences: Earth Surface Dynamics, v. 2, p. 1–7, doi:10.5194/esurf-2-1-2014.

Stolle, A. et al., 2019, Protracted river response to medieval earthquakes: Earth Surface Processes and Landforms, v. 44, p. 331–341, doi:10.1002/esp.4517.

Strang, G., 1988, A Framework for Equilibrium Equations: SIAM Review, v. 30, p. 283–297.

Takaku, J., Tadono, T., and Tsutsui, K., 2014, Generation of High Resolution Global DSM from ALOS PRISM: ISPRS - International Archives of the Photogrammetry, Remote Sensing and Spatial Information Sciences, v. XL–4, p. 243–248, doi:10.5194/isprsarchives-XL-4-243-2014.

Whipple, K.X., DiBiase, R.A., and Crosby, B.T., 2013, Bedrock Rivers, *in* Treatise on Geomorphology, Elsevier, p. 550–573, http://linkinghub.elsevier.com/retrieve/pii/B9780123747396002542 (accessed May 2016).